Journal of Molecular Structure 1230 (2021) 129908

Contents lists available at ScienceDirect

Journal of Molecular Structure

journal homepage: www.elsevier.com/locate/molstr

Synthesis, crystal structure, theoretical calculation, spectroscopic and antibacterial activity studies of copper(II) complexes bearing bidentate schiff base ligands derived from 4-aminoantipyrine: Influence of substitutions on antibacterial activity

Hadi Kargar[a,*], Fariba Aghaei-Meybodi[b], Reza Behjatmanesh-Ardakani[b], Mohammad Reza Elahifard[c], Vajiheh Torabi[b], Mehdi Fallah-Mehrjardi[b], Muhammad Nawaz Tahir[d], Muhammad Ashfaq[d], Khurram Shahzad Munawar[e,f]

[a] Department of Chemical Engineering, Faculty of Engineering, Ardakan University, P.O. Box 184, Ardakan, Iran
[b] Department of Chemistry, Payame Noor University, 19395-3697 Tehran, Iran
[c] Department of Metallurgical Engineering, University of Nevada, Reno, NV 89557, United States
[d] Department of Physics, University of Sargodha, Punjab, Pakistan
[e] Department of Chemistry, University of Sargodha, Punjab, Pakistan
[f] Department of Chemistry, University of Mianwali, Mianwali, Pakistan

ARTICLE INFO

Article history:
Received 1 October 2020
Revised 27 December 2020
Accepted 29 December 2020
Available online 7 January 2021

Keywords:
Schiff base complex
X-ray structure
Theoretical calculation
Antibacterial activity

ABSTRACT

A novel series of Cu(II) complexes, including: $[Cu(L^1)_2]$: **C1**, $[Cu(L^2)_2]$: **C2**, $[Cu(L^3)_2]$: **C3**, $[Cu(L^4)_2]$: **C4**, with four bis-N,O-bidentate Schiff base ligands (H**L**^{1}: (*E*)-4-[(2–*hydroxy*-3-*methoxybenzylidene*)*amino*]-1,5-dimethyl-2-phenyl-1,2-dihydro-3*H*-pyrazol-3-one; H**L**^{2}: (*E*)-4-[(2–*hydroxy*-4-*methoxybenzylidene*)*amino*]-1,5-dimethyl-2-phenyl-1,2-dihydro-3*H*-pyrazol-3-one; H**L**^{3}: (*E*)-4-[(2–*hydroxy*-5-*methoxybenzylidene*)*amino*]-1,5-dimethyl-2-phenyl-1,2-dihydro-3*H*-pyrazol-3-one; H**L**^{4}: (*E*)-4-[(2–*hydroxy*-6-*methoxybenzylidene*)*amino*]-1,5-dimethyl-2-phenyl-1,2-dihydro-3*H*-pyrazol-3-one have been synthesized and characterized by elemental analyses, FT-IR, ^{1}H NMR and ^{13}C NMR spectroscopic techniques. Furthermore, the crystal structures of H**L**^{4} and **C2** were determined by single crystal X-ray analysis. Single crystal X-ray analyses, the structure of **C2** confirmed the bidentate coordination mode. The metal center possesses a distorted tetrahedral geometry with bis-N,O donor atoms coordinating from Schiff base ligand. Theoretical calculation of the synthesized compounds were carried out by DFT using B3LYP method with employing the Def2-SVPD (for ligands) and Def2-SV(P) (for complexes) basis sets. Calculated data are in good accordance with the experimental investigations. The in vitro biological activities of the synthesized ligands and their copper(II) complexes were evaluated against *Staphylococcus aureus* and *Escherichia coli*. The activity data showed that the metal complexes have a promising biological potential comparable with the parent Schiff base ligands against bacterial species.

1. Introduction

During the last few decades utmost attention is given to the Schiff base metal complexes due to their consideration as stereochemical models in coordination chemistry, their easy mode of preparation and structural diversity. Schiff bases complexes behaves as active anticancer drugs with enhanced potential as compared to free ligands [1,2]. The most promising advancement in the field of medicinal chemistry is due to the introduction of heterocyclic compounds which performed an important function in regulating the biological activities. Among these heterocyclic moieties antipyrines played the leading roles in biotransformation of drugs within the human body and also showed positive response in monitoring the patients with chronic liver illness (Hepatitis B virus (HBC), hepatitis C virus (HCV) and alcohol related disease) [3,4].

4-aminoantipyrine, through the condensation reaction with various types of organic reagents such as aldehydes, ketones, thiosemicarbazides, carbazides, and similar compounds, is able to form flexible ligand systems which are able to coordinate to a variety of metals [5]. Schiff bases derived from 4-aminoantipyrine

* Corresponding authors.
E-mail addresses: h.kargar@ardakan.ac.ir, hadi_kargar@yahoo.com (H. Kargar).

https://doi.org/10.1016/j.molstruc.2021.129908
0022-2860/

and their respective transition metal complexes exhibit potential biological activities like antibacterial, antifungal, antitumor, anti-inflammatory, anti-leishmanial and antiviral [6-10]. These derived Schiff bases act as corrosion inhibitors of mild steel in acidic media and also showed solvatochromism depending on polarity of the solvent [11,12].

From coordination point of view the Schiff bases of 4-aminoantipyrine has an advantage that it has two potential donor sites and is likely to form three types of compounds with metal ions [13] viz. (i) chelates utilizing both donor atoms, (ii) amine salts, using only the amino nitrogen atoms and (iii) two types of complexes, i.e., coordination only from the carbonyl oxygen atom or amino nitrogen atom. It has been revealed from literature that there are drastic changes in the biological properties of ligands took place on chelation with metals [14-16].

As a consequence, 4-aminoantipyrine drew attention of researchers to do theoretical studies revealing its denticity and binding modes. However, no work has been done on the influence of substitution on the Schiff bases derived from 4-aminoantipyrine on their biological activities [17].

Copper is considered a very important metal from the coordination point of view and it plays a key role in variety of biological process like electron transfer reactions for the activation of many antitumor moieties. It is also an essential micronutrient, required in small quantities for performing various functions in the human body. It also acts as co-factor for many enzymes which are involved in oxidative metabolism [18,19]. Copper complexes with 4-aminoantipyrines derivatives have ability to intercalate with nitrogenous bases of DNA and in addition to this Cu(II) is also involved in the causation and treatment of cancer [20-22]. A brief overview of literature explored that the theoretical calculations are very useful for predicting the molecular properties and providing insight into the structural investigations of the compounds [23-27]. There are only a few reported structure involving the Cu(II) complexes bearing N,O-bidentate Schiff base ligands derived from 4-aminoantipyrine in cambridge structural database [28,29].

Keeping in mind these facts we have synthesized and characterized a new series of Cu(II) complexes with the heterocyclic Schiff base derived by the condensation of 4-aminoantipyrine with methoxy substituted salicylaldehydes (H**L**^{1}-H**L**^{4}). Theoretical calculation of the synthesized compounds were carried out by DFT using B3LYP method with employing the Def2-SVPD basis set. Further these synthesized compounds were tested against various strains of bacteria to explore the impact of substitution on the bacterial activity.

2. Experimental

2.1. Physical measurements

Microanalysis of the complexes was done using a Heraeus CHN–O-FLASH EA 1112 elemental analyzer. IR spectra were recorded on a FT-IR Prestige 21 spectrophotometer from 400–4000 cm^{-1} using KBr pellets. ^{1}H NMR spectroscopy in $CHCl_3$-*d* (400 MHz, Bruker), ^{13}C NMR spectroscopy in $CHCl_3$-*d* (100 MHz, Bruker) was carried out by using tetramethylsilane (TMS) as internal standard. Chemical shifts for proton resonances are reported in ppm (δ) relative to tetramethylesilane and $CHCl_3$-*d*.

2.2. Syntheses of schiff base ligands (H**L**^{n}) (**n = 1–4**)

For the preparation of bidentate Schiff base ligands, H**L**^{n}, a mixture of 4-aminoantipyrine and the respective salicylaldehyde (3-methoxysalicylaldehyde = H**L**^{1}, 4-methoxysalicylaldehyde = H**L**^{2}, 5-methoxysalicylaldehyde = H**L**^{3} and 6-methoxysalicylaldehyde = H**L**^{4}) with 1:1 stoichiometric ratio was dissolved in EtOH. The mixture was stirred for about 1 h at room temperature to give a clear yellow solution. After that the solution was allowed to slowly evaporate for a period of 5 days to give the products in pure form (H**L**^{1}-H**L**^{3}) and yellow prism-shaped crystals (H**L**^{4}) suitable for an X-ray crystal structure analyses. The elemental analyses, ^{1}H NMR, ^{13}C NMR and IR data, clearly confirmed their composition. The synthesis of the ligands is illustrated in Scheme 1.

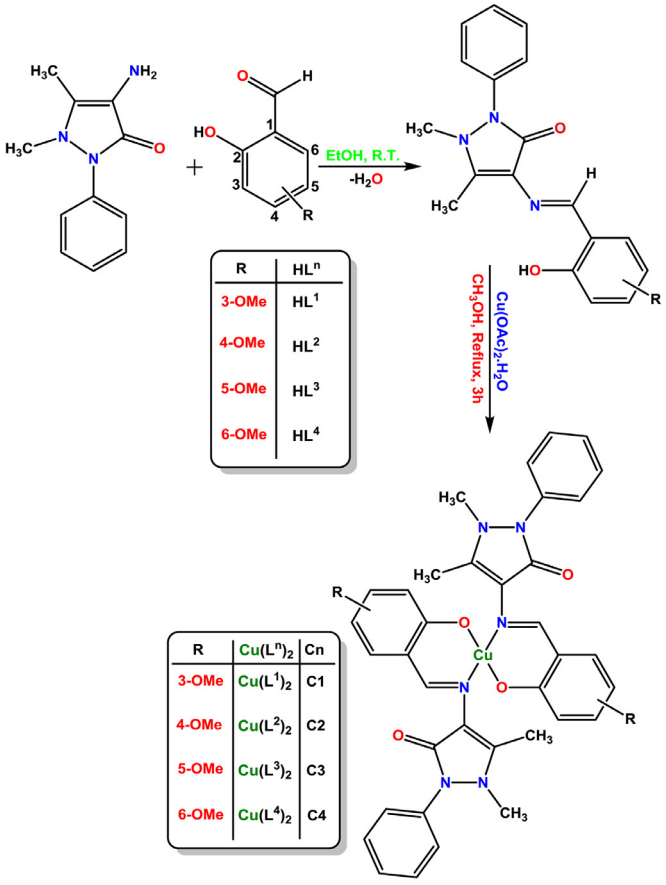

Scheme 1. The synthesis pathways of the H**L**^{1}–H**L**^{4} ligands and **C1–C4** complexes.

H**L**^{1}; (*E*)−4-[(2-*hydroxy*-3-*methoxybenzylidene*)*amino*]−1,5-dimethyl-2-phenyl-1,2-dihydro-3*H*-pyrazol-3-one, Yield: 89%. Calculated for $C_{19}H_{19}N_3O_3$: C 67.64, H 5.68, N 12.46%. Analysis found: C 67.51, H 5.70, N 12.37. IR (KBr, cm^{-1}): ν (*C = O*) 1662, ν (*C = N*) 1599, ν (C–O) 1138. ^{1}H NMR ($CDCl_3$, 400 MHz, 298 K) δ/ppm: 2.44 (s, 3H, –CH_3–C); 3.21 (s, 3H,–CH_3–N); 3.95 (s, 3H, –CH_3–O); 6.86 (t, ^{3}J = 7.8 Hz, H_b); 6.95 (dd, ^{3}J = 7.8 Hz, ^{4}J = 1.5 Hz, H_c); 7.01 (dd, ^{3}J = 7.8 Hz, ^{4}J = 1.5 Hz, H_a); 7.35–7.53 (m, 5H, antipyrine ring); 9.83 (s, –CH=*N*, H_i); 13.93 (s, –OH, H_p). ^{13}C NMR ($CDCl_3$, 100 MHz, 298 K) δ/ppm: 10.18; 35.65; 56.06; 113.48; 116.04; 118.49; 120.14; 123.59; 124.65; 127.34; 129.33; 134.32; 148.09; 149.97; 150.40; 160.26; 160.49.

H**L**^{2}; (*E*)−4-[(2-*hydroxy*-4-*methoxybenzylidene*)*amino*]−1,5-dimethyl-2-phenyl-1,2-dihydro-3*H*-pyrazol-3-one, Yield: 83%. Calculated for $C_{19}H_{19}N_3O_3$: C 67.64, H 5.68, N 12.46%. Analysis found: C 67.53, H 5.65, N 12.51. IR (KBr, cm^{-1}): ν (*C = O*) 1651, ν (*C = N*) 1593, ν (C–O) 1136. ^{1}H NMR ($CDCl_3$, 400 MHz, 298 K) δ/ppm: 2.42 (s, 3H, –CH_3–C); 3.17 (s, 3H,–CH_3–N); 3.84 (s, 3H, –CH_3–O); 6.48 (dd, ^{3}J = 9.2 Hz, ^{4}J = 2.4 Hz, H_b); 6.48 (d, ^{4}J = 2.4 Hz, H_c); 7.28 (d, ^{3}J = 9.2 Hz, H_a); 7.33–7.53 (m, 5H, antipyrine ring); 9.77 (s, –CH=*N*, H_i); 13.77 (s, –OH, H_p). ^{13}C NMR ($CDCl_3$, 100 MHz, 298 K) δ/ppm: 10.32; 35.89; 55.40; 101.14;

Table 1
Crystal data and structure refinement parameters for H**L**^{4} and **C2** compounds.

Identification code	H**L**^{4}	**C2**
Chemical formula	$C_{19}H_{19}N_3O_3$	$C_{38}H_{36}CuN_6O_6$
Formula weight	337.37	736.27
Temperature (K)	296	296
Wavelength (Å)	0.71073	0.71073
Crystal system	Monoclinic	Triclinic
Space group	$P2_1/c$	$P\bar{1}$
a (Å)	6.8913(4)	10.7079(4)
b (Å)	28.3676(19)	13.0362(5)
c (Å)	9.3850(8)	14.4214(8)
α (°)	90	105.975(2)
β (°)	119.451(7)	102.344(1)
γ (°)	90	110.267(2)
Volume (Å^3)	1715.7(2)	1705.55(13)
Z	4	2
Calculated Density (Mg/m^3)	1.306	1.434
Absorption coefficient (mm^{-1})	0.09	0.70
F(000)	712	766
Crystal Shape	Prism	Prism
Crystal color	Yellow	Black green
Crystal size (mm)	0.32 × 0.23 × 0.22	0.34 × 0.27 × 0.25
Data Collection		
Diffractometer	Bruker KAPPA APEXII CCD Diffractometer	Bruker KAPPA APEXII CCD diffractometer
Absorption correction	multi-scan (SADABS; Bruker, 2007)	multi-scan (SADABS; Bruker, 2007)
No. of measured, independent and observed [I> 2s(I)] reflections	14,661, 3728, 2564	26,861, 7432, 6320
R_{int}	0.029	0.027
Theta range for data collection	2.429° to 26.998°	1.563° to 26.999°
Index ranges	$-8 \le h \le 8$, $-36 \le k \le 36$, $-11 \le l \le 10$	$-13 \le h \le 13$, $-16 \le k \le 16$, $-18 \le l \le 18$
(sin $\theta/\lambda)_{max}$ ($Å^{-1}$)	0.639	0.639
Refinement		
$R[F^2 > 2\sigma(F^2)]$, w$R(F^2)$, S	0.046, 0.129, 1.04	0.035, 0.101, 1.03
No. of reflections	3728	7432
No. of parameters	230	466
H-atom treatment	H-atom parameters constrained	H-atom parameters constrained
$\Delta\rho_{max}$, $\Delta\rho_{min}$ (e Å^{-3})	0.23, −0.20	0.31, −0.38

106.48; 114.09; 116.66; 124.41; 127.11; 129.27; 133.27; 134.50; 149.41; 160.36; 160.53; 162.67; 162.94.

H**L**^{3}; (*E*)−4-[(2-*hydroxy*-5-*methoxybenzylidene*)*amino*]−1,5-dimethyl-2-phenyl-1,2-dihydro-3*H*-pyrazol-3-one, Yield: 81%. Calculated for $C_{19}H_{19}N_3O_3$: C 67.64, H 5.68, N 12.46%. Analysis found: C 67.75, H 5.72, N 12.51. IR (KBr, cm^{-1}): ν (*C* = *O*) 1653, ν (*C* = *N*) 1573, ν (C–O) 1132. ^{1}H NMR ($CDCl_3$, 400 MHz, 298 K) δ/ppm: 2.43 (s, 3H, –CH_3–C); 3.20 (s, 3H,–CH_3–N); 3.78 (s, 3H, –CH_3–O); 6.88–6.91 (br, 3H, H_a, H_b, H_c); 7.34–7.53 (m, 5H, antipyrine ring); 9.82 (s, –CH=*N*, H_i); 13.87 (s, –OH, H_p). ^{13}C NMR ($CDCl_3$, 100 MHz, 298 K) δ/ppm: 10.31; 35.67; 55.84; 114.95; 116.31; 117.47; 119.20; 119.91; 124.62; 127.32; 129.32; 129.36; 134.33; 149.94; 152.28; 154.63; 160.31.

H**L**^{4}; (*E*)−4-[(2-*hydroxy*-5-*methoxybenzylidene*)*amino*]−1,5-dimethyl-2-phenyl-1,2-dihydro-3*H*-pyrazol-3-one, Yield: 76%. Calculated for $C_{19}H_{19}N_3O_3$: C 67.64, H 5.68, N 12.46%. Analysis found: C 67.60, H 5.70, N 12.50. IR (KBr, cm^{-1}): ν (*C* = *O*) 1639, ν (*C* = *N*) 1595, ν (C–O) 1136. ^{1}H NMR ($CDCl_3$, 400 MHz, 298 K) δ/ppm: 2.42 (s, 3H, –CH_3–C); 3.18 (s, 3H,–CH_3–N); 3.84 (s, 3H, –CH_3–O); 6.37 (d, ^3J = 8.3 Hz, H_c); 6.56 (d, ^3J = 8.3 Hz, H_a); 7.23 (t, ^3J = 8.3 Hz, H_b); 7.32–7.52 (m, 5H, antipyrine ring); 10.22 (s, –CH=*N*, H_i); 14.24 (s, –OH, H_p). ^{13}C NMR ($CDCl_3$, 100 MHz, 298 K) δ/ppm: 10.34; 35.83; 55.62; 100.62; 109.51; 109.74; 116.99; 124.41; 127.07; 129.24; 132.90; 134.53; 149.67; 157.25; 160.04; 160.39; 162.29.

2.3. Syntheses of the copper(II) complexes

In order to synthesize the copper(II) complexes [Cu(**L**^{n})$_2$] (**C1–C4**), where **L**^{n}=**L**^{1}**–L**^{4} are bidentate Schiff base ligands (H**L**^{n}), the metal precursor Cu(OAc)$_2$.H$_2$O (0.200 g, 1 mmol) was added to a hot methanolic solution (30 mL) of the corresponding ligand H**L**^{n} (0.675 g, 2.0 mmol) the resultant mixture was refluxed for 3 h and then the precipitates were filtered off, washed thoroughly with methanol and dried in air. Black green crystals of **C2** suitable for X-ray measurements were obtained from methanol solution by slow evaporation. The synthesis of the complexes is illustrated in Scheme 1.

C1; [Cu(L^1)$_2$], Yield: 81%. Calculated for $C_{38}H_{36}CuN_6O_6$: C 61.99, H 4.93, N 11.41%. Analysis found: C 61.87, H 4.97, N 11.52. IR (KBr, cm^{-1}): ν (*C* = *O*) 1658, 1604 ν (*C* = *N*) 1587, ν (C–O) 1215.

C2; [Cu(L^2)$_2$], Yield: 78%. Calculated for $C_{38}H_{36}CuN_6O_6$: C 61.99, H 4.93, N 11.41%. Analysis found: C 62.07, H 4.86, N 11.37. IR (KBr, cm^{-1}): ν (*C* = *O*) 1658, 1610 ν (*C* = *N*) 1587, ν (C–O) 1247.

C3; [Cu(L^3)$_2$], Yield: 73%. Calculated for $C_{38}H_{36}CuN_6O_6$: C 61.99, H 4.93, N 11.41%. Analysis found: C 62.05, H 4.98, N 11.47. IR (KBr, cm^{-1}): ν (*C* = *O*) 1656, 1622 ν (*C* = *N*) 1579, ν (C–O) 1249.

C4; [Cu(L^4)$_2$], Yield: 69%. Calculated for $C_{38}H_{36}CuN_6O_6$: C 61.99, H 4.93, N 11.41%. Analysis found: C 61.88, H 4.95, N 11.45. IR (KBr, cm^{-1}): ν (*C* = *O*) 1664, 1608 ν (*C* = *N*) 1572, ν (C–O) 1246.

2.4. Computational methods

Theoretical calculations involving geometry optimization in the gas and solution phases, vibrational frequencies, and NMR chemical shifts of ligands and complexes were performed with the Gaussian 09 package [30] at B3LYP level of theory [31]. The solution phase was modeled by using IEFPCM with considering the solvent [32]. The standard Def2-SVPD and Def2-SV(P) basis set [33] were used for ligands and complexes, respectively. Geometry optimizations were tested by frequency analysis to be sure that they are in the local minimum of potential energy surface (PES). The results showed no imaginary frequency. The ^{1}H and ^{13}C NMR magnetic isotropic shielding tensors were calculated by the standard Gauge-Independent Atomic Orbital (GIAO) approach in the solution phase [34]. Chemical shift values of H**L**^{1}–H**L**^{4} ligands are calculated by using B3LYP/Def2-SVPD level and IEFPCM model as implicit model of solvent and compared with experimental data in chloroform. The same solvent was used for all IEFPCM calculations for ligands, complexes and TMS. Chemical shifts were calculated by subtracting the appropriate isotopic part of the shielding tensor from that of TMS $\delta_i = \sigma_{TMS}$ - σi. The isotropic shielding constants for TMS calculated in the solution phase at the B3LYP/Def2-SVPD level of theory were equal to 31.54 ppm and 188.22 ppm for the ^{1}H nuclei and the ^{13}C nuclei, respectively.

2.5. Crystallographic methods

The X-ray diffraction measurement of H**L**^{4} and **C2** compounds were carried out on Bruker Kappa APEXII CCD X-ray diffractometer with graphite monochromated Mo-Kα radiation (λ = 0.71073 Å). The yellow and black green single crystals of H**L**^{4} and **C2** suitable for X-ray analysis were obtained from methanol solution and mounted on a glass fiber for data collection on Bruker Apex-II software [35]. The structures were solved by direct methods and subsequent difference fourier maps on SHELXS97 [36] and then refined on F^2 by a full-matrix least-squares procedure using anisotropic displacement parameters. Atomic factors are from the international tables for X-ray Crystallography [37]. All non-hydrogen atoms were refined with anisotropic displacement parameters. Hydrogen atoms were placed in ideal positions and refined as riding atoms with relative isotropic displacement parame-

ters. All refinements were performed using the SHELXL-2018/3 and WinGX-2014.1 programs [38,39]. The method to collect data was ω-scans and integrated using Bruker SAINT [40] software package. The crystallographic illustrations for H**L**^{4} and **C2** were prepared using ORTEP-3 [41] and platon [42]. Experimental parameters pertaining to single-crystal X-ray analysis of compounds are given in Table 1.

2.6. Antimicrobial activity

In *vitro* antibacterial activities of the Schiff base ligands and their copper(II) complexes were evaluated against *Escherichia coli* (*E. coli*) ATCC 25,922 and *Staphylococcus aureus (S. aur)* ATCC 25,923, a common referenced gram-negative and gram-positive bacteria, respectively. The Minimum Inhibitory Concentration (MIC), the lowest level of antimicrobial agent that greatly inhibits the growth of a microorganism, and Minimum Bactericidal Concentration (MBC), the lowest level of antimicrobial agent resulting in microbial death, were determined by dilution methods. In 96-well plates the concentrations of 1024, 512, 256, 128, 64, 32, 16, 8, 4 and 2 μg/mL of free ligands and their complexes accompany with 5 $\times$ 10^5 CFU/ml of test strains (0.5 McFarland) suspended in Muller-Hinton broth (MHB) were run simultaneously. It was also included one growth control (MHB) and one sterility control (MHB + compound). Internal standard, Streptomycin, was used for comparison under similar condition. After incubation at 37 °C for 18–24 h, the MIC for each tested substance was indicated by the presence of a white "pellet" on the well bottom. The dilution representing the MIC and two more concentrated suspensions were plated and enumerated to determine viable CFU/ml as MBC value. It is the lowest concentration of a substance necessary to achieve a bactericidal effect that demonstrates a pre-determined reduction (99.9%) in CFU/ml when compared to the MIC dilution.

3. Results and discussion

3.1. Syntheses

Condensation of 4-aminoantipyrine with equimolar amounts of the respective methoxysalicylaldehyde leads to the formation of an important class of the bidentate Schiff base ligands. The Schiff base ligands H**L**^{1}, H**L**^{2}, H**L**^{3} and H**L**^{4} were prepared by the reaction of 4-aminoantipyrine with the corresponding 3-methoxysalicylaldehyde, 4-methoxysalicylaldehyde, 5-methoxysalicylaldehyde and 6-methoxysalicylaldehyde in nearly 76–89% yield in ethanol. Crystal of ligand H**L**^{4}, suitable for X-ray structure determination, were crystallized from ethanol by slow evaporation of the solvents at room temperature over several days. Treatment of the Schiff base ligands H**L**$^{1-4}$ with the respective $Cu(OAc)_2.H_2O$, in a 2:1 ratio under reflux condition led to the copper(II) complexes (**C1–C4**). Crystals of complex **C2** suitable for X-ray diffraction could be isolated from methanol after slow evaporation of the solvent over a period of 5 days. The spectroscopic data is in good agreement with the chemical formula proposed for Schiff base complexes. The synthetic procedure of Schiff base ligands and their copper complexes is presented in Scheme 1.

3.2. Crystal structures of H*L*^{4} and *C2* compounds

In the 4-{(E)-[(2-H*ydroxy*-6-*methoxyphenyl*)*methylidene*]amino}−1,5-dimethyl-2-phenyl-1,2-dihydro-3H-pyrazol-3-one (Fig. 1, Table 1), 3-methoxyphenol group A (C1-C7/O1/O2), 5-methyl-4-(methyleneamino)−1H-pyrazol-3(2H)-one group B(C8-C12/N1/N2/O3) and phenyl ring C (C14-C19) is planar with r. m. s deviation of 0.0599, 0.0270 and 0.0062 Å, respectively. The dihedral angle between A/B, A/C and B/C is 4.05 (8)°, 50.4 (6)° and 54.4 (6)°, respectively. The dihedral angle between 3-methoxyphenol group A (C1-C7/O1/O2) and 5-methyl-4-(methyleneamino)−1H-pyrazol-3(2H)-one group B(C8-C12/N1/N2/O3) shows that these groups are almost parallel. The C-atom of methyl group attach to the ring N-atom of 5-methyl-4-(methyleneamino)−1H-pyrazol-3(2H)-one group is at the distance of −0.4819 (3) Å from least square plane of group B. There exists a strong O–H···N intramolecular bonding between hydroxyl group of phenol moiety and N-atom of interact with N-atom of 2-(iminomethyl)−3-methoxyphenol group to form S(6) loop as shown in Fig. 2 and given in Table 2. There exists another intramolecular C–H···O bonding to form

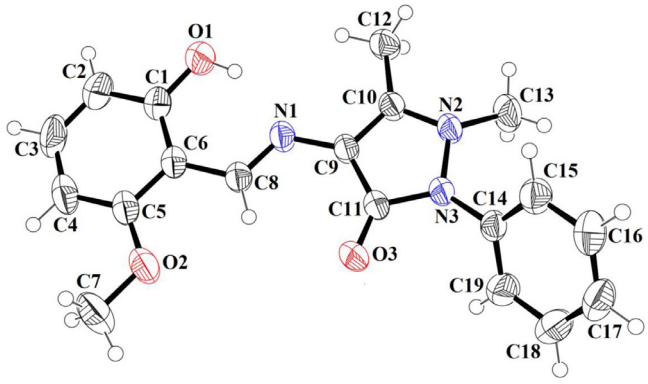

Fig. 1. ORTEP diagram of H**L**^{4} drawn at the probability level of 50% with H-atoms are shown by small circles of arbitrary radii.

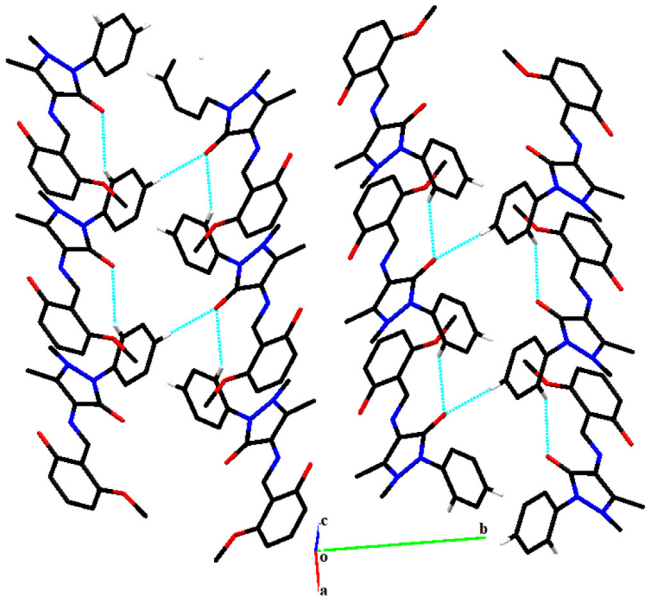

Fig. 2. Packing diagram of H**L**^{4}. H-atoms not involve in H-bonding are omitted for clarity.

Table 2
Hydrogen-bond geometry (Å,°) and C–H···Cg interaction for H**L**^{4}.

D—H···*A*	*D*—H	H···*A*	*D*···*A*	*D*—H···*A*
O1—H1···N1	0.82	1.82	2.5539 (18)	148
C8—H8···O3	0.93	2.40	3.055 (2)	128
C15—H15···O3^{i}	0.93	2.64	3.283 (2)	127
C17—H17···O3^{ii}	0.93	2.56	3.444 (1)	160
C*—H···*Cg	***C*—H**	**H···*Cg***	***C*···*Cg***	***C*—H···*Cg***
C12—H12A···Cg2^{i}	0.96	2.89	3.512(2)	123
C19—H19···Cg2^{iii}	0.96	2.85	3.476(2)	126

Symmetry code: (i) x − 1, y, z, (ii)−1 + x, ½-y, −1/2 + z), (iii) x − 1, y, z-1, where Cg2 is the centroid of phenyl ring (C1-C6).

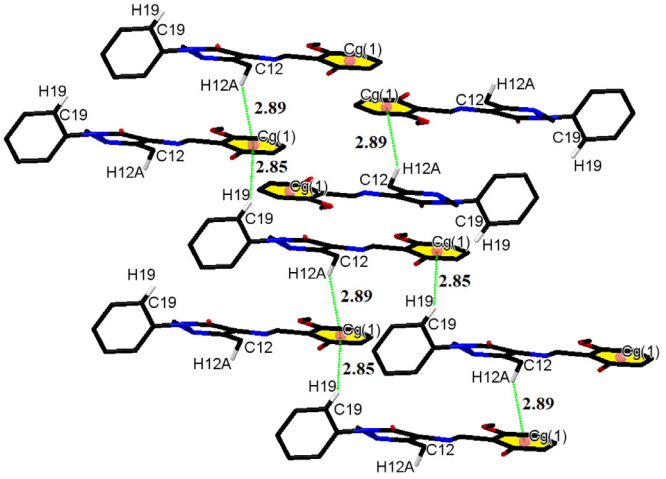

Fig. 3. Graphical repsentation of C–H…π interaction for **HL^4**. H-atoms not involved in C–H…π interaction are omitted for clarity. Distances shown are measured in Å.

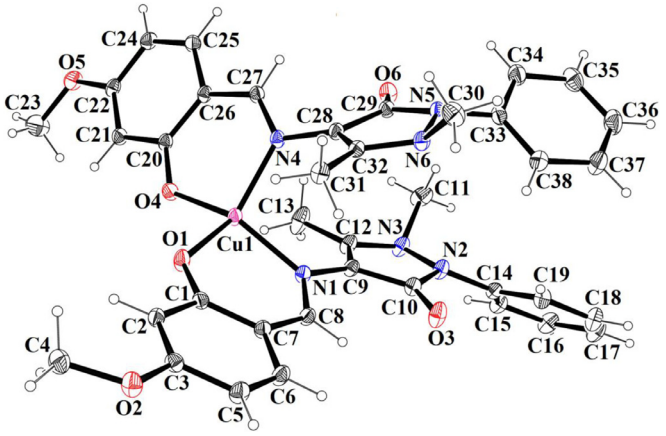

Fig. 4. ORTEP diagram of **C2** drawn at the probability level of 20% with H-atoms are shown by small circles of arbitrary radii.

another S6 loop, where CH is from o-cresol moiety and O-atom is from 1H-pyrazol-3(2H)-one moiety. The molecules are connected with each other through C15-H15···O3^{i} bonding to form infinite chain lying along the a-axis, where CH is from benzene ring attach to 2,3-dihydro-1H-pyrazole ring and O-atom is from 1H-pyrazol-3(2H)-one moiety C. The chains are further interlinked by C17-H17…O3^{ii} bonding. Weak C–H-Cg interaction is also present, resulting in a 2D sheet lying in the ac-plane. This weak interaction helps in further stabilization of crystal packing with C–Cg distance ranges from 3.476(2) Å to 3.512(2) Å as shown in Fig. 3 given in Table 2, where Cg is centroid of phenyl ring (C1-C6).

In the bis(3–methoxy-6-((1-(4–1,5-dimethyl-2-phenyl-1,2-dihydro-3H-pyrazol-3-one)imino)methyl)phenolato)-copper(II) **(C2)** (Fig. 4, Table 1), coordination sphere around the central Cu-atom consists of two N-atoms and two O-atoms with both ligands chelating the central Cu-atom. The chelating nitrogen atoms (N1/N4) are at the distance of 1.9611 (2) and 1.9579 (2) Å, respectively from central Cu-atom whereas the chelating oxygen atoms (O1/O4) are at the distance of 1.8938 (2) and 1.8912 (1) Å, respectively from central Cu-atom. The bond angles in the coordination spheres ranges from 93.04 (7)° to 101.40 (7)°, the dihehral angle between (O4-Cu1-N4) and (O1-Cu1-N1) planes is 53.5 (5)° thus form a distorted tetrahedral geometry. In the first chelating ligand

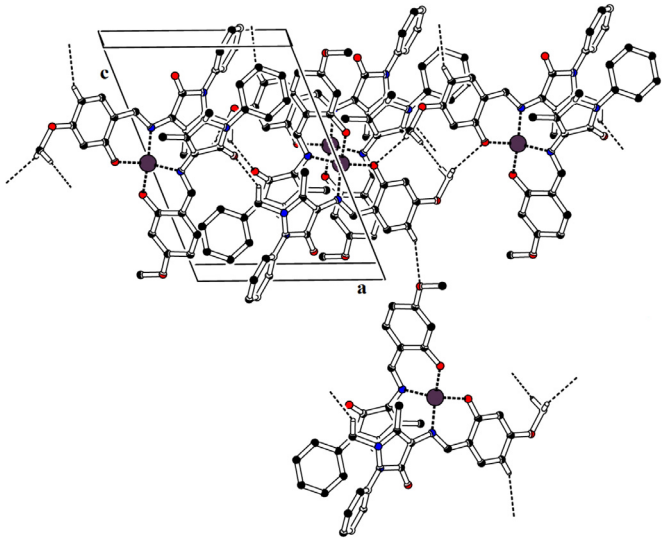

Fig. 5. Packing diagram of **C2** with H-atoms not involve in H-bonding are omitted for clarity.

(C1-C19/N1-N3/O1-O3), the (Z)−3-aminoprop-1-en-1-ol group A (C1/C7/C8/N1/O1) and 3-methoxyphenol group B (C1-C7/O2) is planar with r. m. s deviation of 0.0369 and 0.0404 Å, respectively with dihedral angle of 3.6 (8)° between group A and B. This dihedral angle shows that group A and B are almost parallel. The 1H-pyrazol-3(2H)-one moiety C (C9/C10/C12/N2/N3/O3) and phenyl ring D (C14-C19) is planar with r. m. s deviation of 0.0315 and 0.0061 Å, respectively with the dihedral angle C/D of 34.23 (9)° between them. The C-atom of methyl group attach to nitrogen of 1H-pyrazol-3(2H)-one moiety and C-atom of another methyl group attach to carbon atom of 1H-pyrazol-3(2H)-one moiety is at the distance of −0.8639 (4) and 0.0368 (4) Å, respectively from least square plane of moiety C. In the second chelating ligand (C20-C38/N4-N6/O4-O6), the (Z)−3-aminoprop-1-en-1-ol group E (C20/C26/C27/N4/O4) and 3-methoxyphenol group F (C20-C26/O5) is planar with r. m. s deviation of 0.0199 and 0.0252 Å, respectively with dihedral angle of 4.7 (1)° between group E and F. This dihedral angle shows that group E and F are almost parallel but are not exactly similar to first ligand. The 1H-pyrazol-3(2H)-one moiety G (C28/C29/C32/N5/N6/O6) and phenyl ring H (C33-C38) is planar with r. m. s deviation of 0.0425 and 0.0105 Å, respectively with the dihedral angle G/H of 39.61 (9)° between them. The C-atom of methyl group attach to nitrogen of 1H-pyrazol-3(2H)-one moiety and C-atom of another methyl group attach to carbon atom of 1H-pyrazol-3(2H)-one moiety is at the distance of 0.7398 (3) and 0.0279 (1) Å, respectively from least square plane of moiety G. The dihedral angle between similar moieties in chelating ligands is A/E, B/F, C/G and D/H is 59.30 (6)°, 64.79 (5)°, 21.06 (1)° and 62.26 (8)°, respectively. There exists intramolecular C–H···O bonding to for S6 loop, where CH is from (Z)−3-aminoprop-1-en-1-ol group A and O-atom is from 1H-pyrazol-3(2H)-one moiety C. There is another intramolecular C–H···O bonding is oberved that connect two ligands with each other, where CH is from methyl group attach to 1H-pyrazol-3(2H)-one moiety C and O-atom of 1H-pyrazol-3(2H)-one moiety G. The molecules are connected with each other through C–H···O bonding to form 2D sheet lying parallel to the [210] direction as shown in Fig. 5 and given in Table 3. There exists weak C–H-Cg interaction that helps in further stabilization of crystal packing with C–Cg distance ranges from 3.324(3) Å to 3.238(3) Å as given in Table 3, where Cg is the centroid of (C20/C26/C27/O4/Cu1) ring.

Table 3
Hydrogen-bond geometry (Å,°) and C–H-Cg interaction for **C2**.

D—H···*A*	*D*—H	H···*A*	*D*···*A*	*D*—H···*A*
C4—H4*A*···O6^{i}	0.96	2.56	3.503 (3)	166
C4—H4*C*···O1^{ii}	0.96	2.49	3.225 (3)	134
C5—H5···O5^{iii}	0.93	2.57	3.316 (3)	138
C8—H8···O3	0.93	2.25	2.908 (2)	128
C11—H11*A*···O6	0.96	2.47	3.203 (3)	133
C11—H11*B*···O6^{iv}	0.96	2.35	3.171 (3)	144
C19—H19···O3	0.93	2.48	2.942 (3)	111
C19—H19···O3^{v}	0.93	2.61	3.235 (3)	125
C*—H···*Cg	***C*—H**	**H···*Cg***	***C*···*Cg***	***C*—H···*Cg***
C13—H13A···Cg4	0.96	2.96	3.238(3)	98
C13—H13B···Cg4	0.96	2.71	3.238(3)	116
C32—H32C···Cg4^{i}	0.96	2.57	3.324(3)	136

Symmetry codes: (i) $-x + 2, -y + 1, -z + 1$; (ii) $-x + 3, -y + 1, -z + 1$; (iii) $x, y, z - 1$; (iv) $-x + 1, -y, -z + 1$; (v) $-x + 1, -y, -z$, where Cg4 is the centroid of (C20/C26/C27/N4/O4/Cu1) ring.

3.3. Computational results

Optimized geometry of the compounds are shown in Fig. 6. The selected structural parameters of the compounds are collected in Table **S1**. Data show that theoretical data for selected bond lengths and bond angles are in good line with the experimental ones. In addition, root mean square deviation (RMSD) for all bond lengths and all bond angles (except those belong to hydrogen atoms) were calculated for ligand H**L^{4}** and complex **C2** (Table 4). These RMSD values also show that there is a good agreement between theory and experiments. Geometries of compounds in the gas phase were fully optimized at B3LYP level of theory. The coordination geometry of the **C2** complex is distorted tetrahedral.

3.4. ^{1}H NMR, $^{13}C\{^{1}H\}$ nmr spectra

^{1}H NMR spectra of the ligands were recorded in deuterated chloroform ($CDCl_3$). The results are given in Table 5 and the spectra are shown in Figs. **S1-S4**. The spectra display three sharp signals at 2.42–2.44, 3.17–3.21 and 3.78–3.95 ppm with an integration equivalent to three hydrogens corresponding to the $C{-}CH_3$, $N{-}CH_3$ and $O{-}CH_3$ groups, respectively. The absorption peaks of salicylaldehyde ring protons (H_a, H_b and H_c) appeared within the expected range. The broadening in signals for the aromatic protons observed between 6.37 and 7.23 ppm indicates the presence of repeating aromatic units with a different chemical surrounding. The antipyrine aromatic rings give a group of multi signals at 7.32–7.53 ppm. The sharp singlet signals at δ = 9.77–10.22 ppm are attributed to the H_i-C = *N*- proton of imine. The OH hydrogen for H**L^{1}**–H**L^{4}** resonates at δ = 13.93, 13.77, 13.87 and 14.24 ppm as a sharp singlet, respectively.

The ^{13}C NMR spectra were recorded in $CDCl_3$ solvent. The results are given in Table 6 and the spectra are shown in Figs. **S5-S8**. The signals due to methyl carbon are observed around 10–56 ppm. The signals that appeared in region δ = 100.6–149.6 ppm are assigned to aromatic and pyrazoline ring carbons. The signals at δ = 154.6–162.9 ppm are assigned to the carbon of *C* = *O* and the carbon of *C* = *N*, respectively. For comparison, the NMR chemical shifts (δ) have been calculated in the solution phase at the B3LYP/Def2-SVPD level of theory for the H**L^{1}**-H**L^{4}** ligands. The experimental and calculated ^{1}H and ^{13}C NMR chemical shifts (δ) of the ligands are collected in Tables 5 and 6. The differences between the theoretical and experimental chemical shifts for ligands are lower than 4%. The experimental chemical shifts are in good consistency with the calculated chemical shifts.

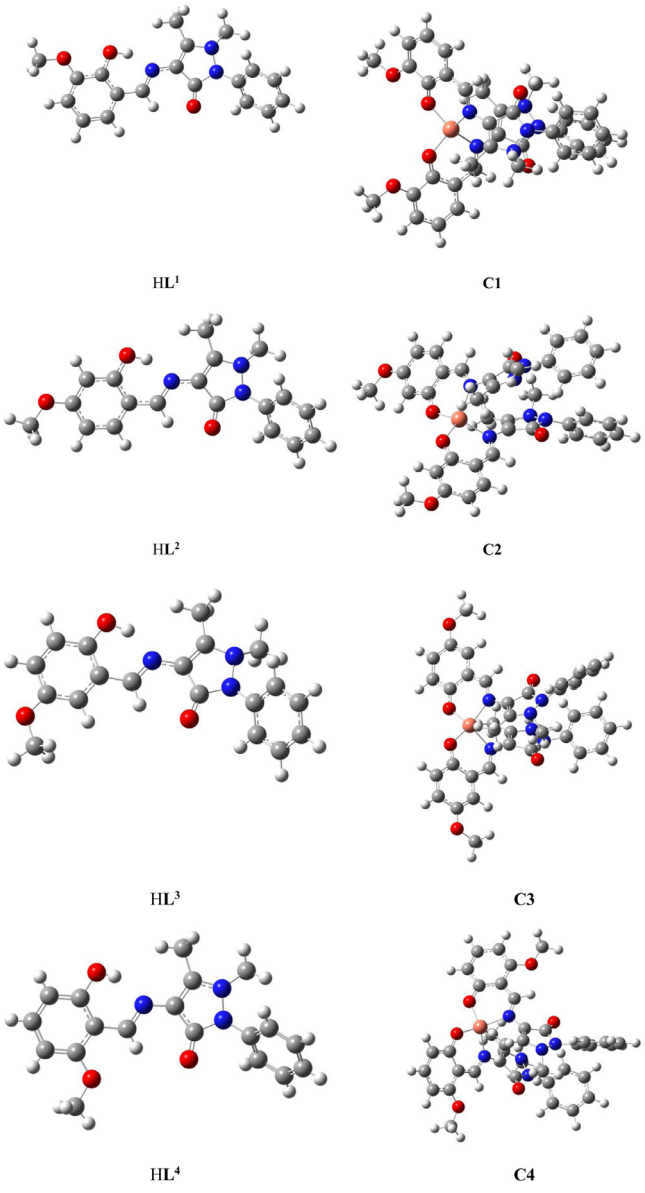

Fig. 6. Optimized structures of compounds.

3.5. FT-IR spectra

The measured FT-IR spectra of the ligands and their corresponding copper(II) complexes are shown in Figs. **S9-S16**. The comparison between the selected bands in the IR spectra of Schiff base ligands and their complexes are presented in Table 7 and Fig. **S17**. In the FT-IR spectra for **C1**-**C4** complexes, the ν (*C* = *O*) remains unmodified, indicating that the exocyclic ketonic oxygen of the antipyrine ring is not involved in the coordination while the ν (*C* = *N*) and ν (C–O) bonds shifted to lower and higher wave numbers, respectively, in comparison with their corresponding free ligands thereby indicating a coordinative interaction between the iminic nitrogen and phenolic oxygen atoms with Cu(II) central metals. Theoretical data for ligands and complexes confirm this subject. The iminic nitrogen and phenolic oxygen coordination could also be confirmed by appearance of weak bands located at the low wavenumbers which assigned to (M–N) and (M–O) at 416–436 cm^{-1} and 530–551 cm^{-1} respectively. The vibrational frequencies of ligands were calculated at B3LYP/Def2-SVPD and vibrational frequencies of complexes were calculated at B3LYP/Def2-SV(P) (two

Table 4
The root mean square deviation (RMSD*) for the bond lengths and bond angles of the **HL^4, C2** compounds.

	HL^4			**C2**		
	Exp	Calc	Δ	Exp	Calc	Δ
Bond lengths						
C = N	1.291(2)	1.291	0	1.304(3), 1.301(2)	1.312, 1.314	0.008, 0.013
C–OH	1.351(2)	1.351	0	1.300(2), 1.302(2)	1.287, 1.289	−0.013,−0.013
C = O	1.2322(19)	1.232	−0.0002	1.219(2), 1.224(2)	1.228, 1.227	0.009, 0.003
C–OCH_3	1.363(2)	1.363	0	1.361(2), 1.360(2)	1.354, 1.354	−0.007,−0.006
N–N	1.3999(19)	1.400	0.0001	1.403(2), 1.406(2)	1.401, 1.400	−0.002, −0.006
Cu1–O1	–	–	–	1.8942(14)	1.9392	0.045
Cu1–O4	–	–	–	1.8915(13)	1.9364	0.0449
Cu1–N4	–	–	–	1.9581(16)	2.0038	0.0457
Cu1–N1	–	–	–	1.9615(16)	2.0086	0.0471
RMSD**	**0.0004**			**0.0193**		
Bond angles						
N4–Cu1–N1	–	–	–	101.40(7)	101.49	0.09
O4–Cu1–O1	–	–	–	93.05(6)	95.89	2.84
O1–Cu1–N4	–	–	–	137.35(7)	142.76	5.41
O4–Cu1–N1	–	–	–	144.73(7)	140.73	−4
O1–Cu1–N1	–	–	–	95.55(7)\	93.33	−2.22
O4–Cu1–N4	–	–	–	94.99(6)	93.98	−1.01
C5–O2–C7	118.33	118.34	0.01	–	–	–
C8–N1–C9	122.53	122.55	0.02	–	–	–
C10–N2–N3	107.35	107.34	−0.01	–	–	–
C10–N2–C13	125.44	125.44	0	–	–	–
N3–N2–C13	118.08	118.08	0	–	–	–
C11–N3–N2	109.74	109.76	0.02	–	–	–
C11–N3–C14	125.98	125.98	0	–	–	–
N2–N3–C14	120.75	120.73	−0.02	–	–	–
O1–C1–C2	118	118.02	0.02	–	–	–
O1–C1–C6	120.83	120.83	0	–	–	–
RMSD***	**0.0238**			**1.3048**		

* RMSD=$\sqrt{\frac{1}{n}\sum_{i}^{n}(X_i^{calc}-X_i^{exp})^2}$, *i*= variable, *n*= number of data, X_i^{calc}= theoretical bond lengths or bond angles, X_i^{exp}= experimental bond lengths or bond angles.
** RMSD calculated for all bond lengths except those containing hydrogen atom.
*** RMSD calculated for all bond angles except those containing hydrogen atom.

Table 5
Characteristic ^{1}H NMR chemical shift values (ppm), peak multiplicity and coupling constant *J* (Hz) for the synthesized compounds recorded in $CDCl_3$.

compound	**-CH_3-C**	**-CH_3-N**	**-CH_3-O**	**H_a**	**H_b**	**H_c**	**antipyrine ring (5 H)**	**H_i**	**H_p**
HL^1	2.44 s (2.49)*	3.21 s (3.21)	3.95 s (4.00)	7.01 dd (7.09) *J* = 7.8;1.5	6.86 t (7.02) *J* = 7.8	6.95 dd (6.97) *J* = 7.8; 1.5	7.35–7.53 m (7.29–7.79)	9.83 s (10.09)	13.93 s (14.43)
HL^2	2.42 s (2.49)	3.17 s (3.18)	3.84 s (3.95)	7.28 d (7.50) *J* = 9.2	6.48 dd (6.50) *J* = 9.2;2.4	6.48 d (6.50) *J* = 2.4	7.33–7.53 m (7.28–7.78)	9.77 s (10.03)	13.77 s (14.37)
HL^3	2.43 s (2.46)	3.20 s (3.21)	3.78 s (3.89)	6.88–6.91br (6.86)	6.88–6.91br (7.01)	6.88–6.91br (7.01)	7.34–7.53 m (7.29–7.79)	9.82 s (10.10)	13.87 s (13.81)
HL^4	2.42 s (2.46)	3.18 s (3.19)	3.84 s (3.97)	6.56 d (6.37) *J* = 8.3	7.23 t (7.43) *J* = 8.3	6.37 d (6.61) *J* = 8.3	7.32–7.52 m (7.29–7.79)	10.22 s (10.44)	14.24 s (14.96)

* The calculated ^{1}H NMR chemical shifts are reported in parenthesis.

Table 6
Characteristic ^{13}C NMR chemical shift values (ppm) for the synthesized compounds recorded in $CDCl_3$.

compound	**-CH_3-C**	**-CH_3-N**	**-CH_3-O**	**aromatic and pyrazoline ring carbons**	**-C–OMe**	**-C–OH**	**-*C = O***	**-*C = N***
HL^1	10.18 (9.01)*	35.65 (32.16)	56.06 (53.56)	113.48–148.09 (109.52–149.33)	149.97 (145.64)	150.40 (148.62)	160.26 (157.27)	160.49 (154.74)
HL^2	10.32 (8.97)	35.89 (32.33)	55.40 (53.87)	101.14–149.41 (97.59–148.83)	160.36 (160.60)	160.53 (160.68)	160.26 (157.32)	162.94 (153.71)
HL^3	10.31 (9.02)	35.67 (32.13)	55.84 (53.36)	114.95–134.33 (109.08–149.23)	149.94 (148.51)	152.28 (153.03)	154.63 (157.31)	160.31 (154.09)
HL^4	10.34 (9.16)	35.83 (32.24)	55.62 (54.37)	100.62–149.67 (95.62–149.02)	157.25 (157.84)	160.04 (160.78)	160.39 (157.43)	162.29 (149.55)

* The calculated ^{13}C NMR chemical shifts are reported in parenthesis.

Table 7
IR spectral data of ligands and their corresponding copper(II) complexes (cm^{-1}).

	HL^1		**C1**		**HL^2**		**C2**		**HL^3**		**C3**		**HL^4**		**C4**	
	Exp	Calc	Exp	Calc	Exp	Calc	Exp	Calc	Exp	Calc	Exp	Calc	Exp	Calc	Exp	Calc
C = N	1593	1652	1587	1507	1593	1653	1587	1644	1579	1664	1573	1638	1595	1652	1572	1631
C–O	1138	1314	1215	1387	1136	1267	1247	1354	1132	1306	1249	1361	1136	1354	1246	1375
M–N	–	–	416	561	–	–	418	539	–	–	420	526	–		436	549
M–O	–	–	551	559	–	–	530	592	–	–	551	561	–		530	570

Table 8
MIC and MBC of the Schiff base ligands and their corresponding Cu(II) complexes.

Compound	MIC (μg/ml)		MBC (μg/ml)	
	E. coli	*S. aur*	*E. coli*	*S. aur*
H**L**^{1}	512	256	–	–
H**L**^{2}	256	128	–	1024
H**L**^{3}	128	64	1024	1024
H**L**^{4}	256	256	–	1024
C1	128	32	512	128
C2	64	32	128	64
C3	64	32	128	64
C4	64	64	128	128
Streptomycin	8	4	32	16

different basis sets were used: the smaller basis set of Def2-SV(P) for complexes which have more atoms than ligands, and the larger basis set of Def2-SVPD for ligands). Some of the most important experimental and calculated frequencies for ligands and complexes are collected in Table 7. The calculated DFT frequencies are in close agreement with the experimental values.

3.6. Antibacterial activities

Using MIC and MBC measurements, the in vitro antibacterial activities of the Schiff base ligands and their copper(II) complexes were screened. The results (Table 8) show the significant antibacterial activity of all complexes against both *S. aur* and *E. coli*, while the free ligands resulted in a moderate activity under the same experimental conditions. All tested compounds, however, show greater bacterial activities against gram positive than gram negative strains. Having thicker peptidoglycan layer, gram positive bacteria absorb antibiotics and cleaning products easily. However, owing to thin peptidoglycan layer, gram negative bacteria are protected from certain physical assaults because they do not absorb foreign materials that surround it.

Dislocating only the methoxy site, a wide range of inhibitory effect of the synthesized Schiff base ligands (MIC values in 128–512 μg/mL against *E. coli* and 64–512 μg/mL against *S. aur*) on the growth of the strains appeared eccentrically; a high influence of substitutions on antibacterial activity. It is claimed that the formation of a hydrogen bond with the active centres of cell constituents disturbs/inhibits the normal cell process [43]. Accordingly, the different activity of the free ligands (H**L**^{3} > H**L**^{2} & H**L**^{4} > H**L**^{1}) can be discussed over the ability of methoxy group to form hydrogen bond; in H**L**^{1}, spatial barrier limits the involvement of hydroxy and methoxy groups to form hydrogen bond leading the highest MIC value; in H**L**^{2} and H**L**^{4}, whereas methoxy groups are electron donor substituent reducing their ability, low spatial barrier to hydroxy group leads a moderat antibacterial activity; in H**L**^{3} where methoxy group is an electron acceptor substituent with the lowest spatial barrier, the most antibacterial activity was observed. The MBC results of free ligands, however, show ignorable bactericidal activities.

Compared to their ligands, the complexes provide greater bactericidal activities and inhibitory effects in a small range; MBC and MIC values of 128 and 64 μg/mL against *E. coli* and 64 and 32 μg/mL against *S. aur*, respectively. It can be explained out of coordination bond formation on the basis of Overtone's concept [44] and Tweedy's chelation theory [45]. Coordination reduces the polarity of the central metal ion leading its larger atomic radius and electronegativity that decreases its effective positive charges and facilitates the interaction of complexes with cellular membranes which are highly sensitive towards the charged particle [46]. Moreover, the delocalization of π-electrons over the chelate ring system created by the donor groups during the coordination increases the lipophilicity of the complexes. It boosts their permeation through the lipid layer of the microorganism, thus destroying them more efficiency [47,48].

4. Conclusion

In conclusion, we have succesfuly synthesized a series of Schiff base ligands derived from 4-aminoantipyrine and their copper(II) complexes. The single crystal X-ray structure of **C2**, illustrates that the steric effect imposed by the methyl group has a profound influence on the Cu(II) geometry, rearranging into a distorted tetrahedral geometry. Theoretical calculation results were found to be in good agreement with experimental results. Affecting the ability of salicylaldehyde ring to form hydrogen bond with the active center of cell, the position of methoxy group brings different antimicrobial activity. The in vitro biological screening experiments showed higher activities for the complexes compared to the free Schiff base ligands.

Compliance with ethical standards

Conflict of interest: The authors declare that they have no conflict of interest.

Author's statement

We would like to make an statement about the author's main contribution: HK, FAM and MFM synthesized all the compounds, and characterized them by different techniques; RBA and VT designed the model and the computational framework and analysed the data.; MRE was responsible for biological data acquisition and analysis; MNT, MA and KSM collected the single-crystal X-ray diffraction data and determined the structures. HK wrote the manuscript with input from all authors. All authors discussed the results and commented on the manuscript.

Declaration of Competing Interest

The authors declare that they have no conflict of interest.

Acknowledgement

The support of this work by Ardakan University and Payame Noor University are gratefully acknowledged.

Appendix A. Supplementary data

CCDC No. 2031,693 (for **C2**) and CCDC No. 2031,694 (for H**L**^{4}) contain the supplementary crystallographic data for this contribution. Copies of the data may be obtained free of charge on application to CCDC, 12 Union Road, Cambridge CB2 1 EB, UK (Fax: +44–1223–336–033; E-mail: deposit@ccdc.cam.ac.uk or http://www.ccdc.cam.ac.uk).

References

[1] N. Uddin, F. Rashid, S. Ali, S.A. Tirmizi, I. Ahmad, S. Zaib, M. Zubair, P.L. Diaconescu, M.N. Tahir, J. Iqbal, A. Haider, Synthesis, characterization, and anticancer activity of Schiff bases, J. Biomol. Struct. Dyn. 38 (11) (2020) 3246–3259.
[2] S.N. Mbugua, N.R. Sibuyi, L.W. Njenga, R.A. Odhiambo, S.O. Wandiga, M. Meyer, R.A. Lalancette, M.O. Onani, New Palladium (II) and Platinum (II) Complexes Based on Pyrrole Schiff Bases: synthesis, Characterization, X-ray Structure, and Anticancer Activity, ACS omega, 5 (25) (2020) 14942–14954.
[3] P.S. Wissel, Dose dependent suppression of hepatic cytochrome P-450 content by doxorubicin and mitomycin-C: correlation with antipyrine biotransformation, Life Sci 42 (11) (1988) 1139–1145.

[4] A. Grieco, A. Matera, P.D. Rocco, S. Marcoccia, A. Giancaterini, B. Alfei, G. Addolorato, F. Varlese, G. Gasbarrini, Plasma levels of fibronectin in patients with chronic viral and alcoholic liver disease, Hepatogastroenterology 45 (23) (1998) 1731–1736.

[5] N. Raman, S.J. Raja, A. Sakthivel, Transition metal complexes with Schiff-base ligands: 4-aminoantipyrine based derivatives–a review, J. Coord. Chem. 62 (5) (2009) 691–709.

[6] V. Ossai, A.P. Obiefuna, B.C. Laraps, O.U. Okenyeka, J.C. Ezeorah, N. Dege, A. Ibezim, M. Lutter, K. Jurkschat, N.L. Obasi, Crystal structural and in silico studies of Schiff bases derived from 4-aminoantipyrine, Solid State Sci 106 (2020) 106293.

[7] A.A.H. Abdel-Rahman, A.H.A. Ahamed, M.M.M. Ramiz, Synthesis and anti-hbv activity of 4-aminoanti-pyrine derivatives, Chem. Heterocycl. Comp. 46 (2010) 72–78.

[8] P.M.P. Santos, A.M.M. Antunes, J. Noronha, E. Fernandes, A.J.S.C. Vieira, Scavenging activity of aminoantipyrines against hydroxyl radical, Eur. J. Med. Chem. 45 (6) (2010) 2258–2264.

[9] P.R. Chavan, K.M. Hosamani, Microwave-assisted synthesis, computational studies and antibacterial/anti-inflammatory activities of compounds based on coumarin-pyrazole hybrid, R. Soc. open sci. 5 (2018) 172435.

[10] R. Teran, R. Guevara, J. Mora, L. Dobronski, O. Barreiro-Costa, T. Beske, J. Pérez-Barrera, R. Araya-Maturana, P. Rojas-Silva, A. Poveda, J. Heredia-Moya, Characterization of Antimicrobial, Antioxidant, and Leishmanicidal Activities of Schiff Base Derivatives of 4-Aminoantipyrine, Molecules 24 (15) (2019) 2696–2716.

[11] N.C. Okey, N.L. Obasi, P.M. Ejikeme, D.T. Ndinteh, P. Ramasami, E.M. Sherif, E.D. Akpan, E.E. Ebenso, Evaluation of some amino benzoic acid and 4-aminoantipyrine derived Schiff bases as corrosion inhibitors for mild steel in acidic medium: synthesis, experimental and computational studies, J. Mol. Liq. 315 (2020) 113773.

[12] A. Upadhyay, P.K. Kar, S. Dash, A spectrophotometric study of impact of solvent, substituent and cross-conjugation in some 4-aminoantipyrine based Schiff bases, Spectrochim. Acta, Part A 233 (2020) 118231.

[13] M.E. Hossain, M.N. Alam, J. Begum, A.M. Akbar, M. Nazimuddin, F.E. Smith, R.C. Hynes, The preparation, characterization, crystal structure and biological activities of some copper(II) complexes of the 2-benzoylpyridine Schiff bases of S-methyl- and S-benzyldithiocarbazate, Inorg. Chim. Acta 249 (1996) 207–213.

[14] H.F.G. Barbosa, M. Attjioui, A.P.G. Ferreira, B.M. Moerschbacher, E.T.G. Cavalheiro, New series of metal complexes by amphiphilic biopolymeric Schiff bases from modified chitosans: preparation, characterization and effect of molecular weight on its biological applications, Int. J. Biol. Macromol. 145 (2020) 417–428.

[15] B. Macias, I. Garcia, M.V. Villa, J. Borras, M. Gonzalez-Alvarez, A. Castineiras, Oxidative DNA damage of mixed copper(II) complexes with sulfonamides and 1,10-phenanthroline: crystal structure of [Cu(N-quinolin-8-yl-p-toluenesulfonamidate)$_2$(1,10-phenanthroline)], J. Inorg. Biochem. 96 (2–3) (2003) 367–374.

[16] S. Chandra, L.K. Gupta, EPR, mass, IR, electronic, and magnetic studies on copper(II) complexes of semicarbazones and thiosemicarbazones, Spectrochim. Acta, Part A 61 (1–2) (2005) 269–275.

[17] P.M. Selvakumar, E. Suresh, P.S. Subramanian, Synthesis, spectral characterization and structural investigation on some 4-aminoantipyrine containing Schiff base Cu (II) complexes and their molecular association, Polyhedron 26 (4) (2007) 749–756.

[18] K.D. Karlin, Y. Gultneh, Bioinorganic chemical modeling of dioxygen-activating copper proteins, J. Chem. Ed. 62 (11) (1985) 983–992.

[19] J.A. Halfen, S. Mahapatra, E.C. Wilkinson, S. Kaderli, V.G. Young Jr, L. Que Jr, A.D. Zuberbühler, W.B. Tolman, Reversible cleavage and formation of dioxygen O-O bond within a copper complex, Science 271 (5254) (1996) 1397–1400.

[20] B. Anupama, M. Padmaja, C.G. Kumari, Synthesis, characterization, biological activity and DNA binding studies of metal complexes with 4-Aminoantipyrine Schiff base ligand, E- J. Chem. 9 (1) (2012) 389–400.

[21] S. Sathiyaraj, K. Sampath, R.J. Butcher, R. Pallepogu, C. Jayabalakrishnan, Designing, structural elucidation, comparison of DNA binding, cleavage, radical scavenging activity and anticancer activity of copper (I) complex with 5-dimethyl-2-phenyl-4-[(*pyridin-2-ylmethylene*)-*amino*]-1, 2-dihydro-pyrazol-3-one Schiff base ligand, Eur. J. Med. Chem. 64 (2013) 81–89.

[22] N. Raman, L. Mitu, A. Sakthivel, M.S.S. Pandi, Studies on DNA cleavage and antimicrobial screening of transition metal complexes of 4-aminoantipyrine derivatives of N_2O_2 type, J. Iran. Chem. Soc. 6 (4) (2009) 738–748.

[23] V. Torabi, H. Kargar, A. Akbari, R. Behjatmanesh-Ardakani, H. Amiri-Rudbari, M.N. Tahir, Nickel(II) complex with an asymmetric tetradentate Schiff base ligand: synthesis, characterization, crystal structure, and DFT studies, J. Coord. Chem. 22 (2018) 3748–3762.

[24] H. Kargar, V. Torabi, A. Akbari, R. Behjatmanesh-Ardakani, M.N. Tahir, Synthesis, characterization, crystal structure and DFT studies of a palladium(II) complex with an asymmetric Schiff base ligand, J. Mol. Struct. 1179 (2019) 732–738.

[25] H. Kargar, V. Torabi, A. Akbari, R. Behjatmanesh-Ardakani, M.N. Tahir, Synthesis, crystal structure, experimental and theoretical studies of tetradentate N_2O_2 Schiff base ligand and its Ni(II) and Pd(II) complexes, J. Iran. Chem. Soc. 16 (2019) 1081–1090.

[26] H. Kargar, V. Torabi, A. Akbari, R. Behjatmanesh-Ardakani, A. Sahraei, M.N. Tahir, Synthesis, crystal structure, spectroscopic investigations and computational studies of Ni(II) and Pd(II) complexes with asymmetric tetradentate NOON Schiff base ligand, Struct. Chem. 30 (2019) 2289–2299.

[27] H. Kargar, V. Torabi, A. Akbari, R. Behjatmanesh-Ardakani, A. Sahraei, M.N. Tahir, Pd(II) and Ni(II) complexes containing an asymmetric Schiff base ligand: synthesis, x-ray crystal structure, spectroscopic investigations and computational studies, J. Mol. Struct. 1205 (2020) 127642.

[28] G.B. Yan, M.H. Yang, Y.F. Zheng, {4,6-Dichloro-2-[(1,5-*dimethyl*-3-*oxo*-2-*phenyl*-2,3*dihydro*-1H-*pyrazol*-4-*yl*)*iminomethyl*]phenolato-κ^2 N,O}copper(II), Acta Cryst E62 (2006) m3481–m3482.

[29] P.M. Selvakumar, E. Suresh, P.S. Subramanian, Synthesis, spectral characterization and structural investigation on some 4-aminoantipyrine containing Schiff base Cu(II) complexes and their molecular association, Polyhedron 26 (2007) 749–756.

[30] M.J. Frisch, G.W. Trucks, H.B. Schlegel, G.E. Scuseria, M.A. Robb, J.R. Cheeseman, G. Scalmani, V. Barone, B. Mennucci, G.A. Petersson, H. Nakatsuji, M. Caricato, X. Li, H.P. Hratchian, A.F. Izmaylov, J. Bloino, G. Zheng, J.L. Sonnenberg, M. Hada, M. Ehara, K. Toyota, R. Fukuda, J. Hasegawa, M. Ishida, T. Nakajima, Y. Honda, O. Kitao, H. Nakai, T. Vreven, J.A. Montgomery, Jr., J.E. Peralta, F. Ogliaro, M. Bearpark, J.J. Heyd, E. Brothers, K.N. Kudin, V.N. Staroverov, T. Keith, R. Kobayashi, J. Normand, K. Raghavachari, A. Rendell, J.C. Burant, S.S. Iyengar, J. Tomasi, M. Cossi, N. Rega, J.M. Millam, M. Klene, J.E. Knox, J.B. Cross, V. Bakken, C. Adamo, J. Jaramillo, R. Gomperts, R.E. Stratmann, O. Yazyev, A.J. Austin, R. Cammi, C. Pomelli, J.W. Ochterski, R.L. Martin, K. Morokuma, V.G. Zakrzewski, G.A. Voth, P. Salvador, J.J. Dannenberg, S. Dapprich, A.D. Daniels, O. Farkas, J.B. Foresman, J.V. Ortiz, J. Cioslowski, D.J. Fox, GAUSSIAN 09 (Revision D.01), Gaussian, Inc., Wallingford, CT, 2013.

[31] A.D. Becke, Density-functional thermochemistry. III. The role of exact exchange, J. Chem. Phys. 98 (1993) 5648–5652.

[32] J. Tomasi, B. Mennucci, R. Cammi, Quantum mechanical continuum solvation models, Chem. Rev 105 (2005) 2999–3093.

[33] B.P. Pritchard, D. Altarawy, B. Didier, T.D. Gibson, T.L. Windus, A New Basis Set Exchange: an Open, Up-to-date Resource for the Molecular Sciences Community, J. Chem. Inf. Model. 59 (11) (2019) 4814–4820.

[34] J. Gauss, Effects of electron correlation in the calculation of nuclear magnetic resonance chemical shifts, J. Chem. Phys. 99 (1993) 3629–3643.

[35] APEX2, Bruker AXS Inc., Madison, Wisconsin, USA, 2013.

[36] G.M. Sheldrick, A short history of SHELX, Acta Crystallogr A64 (2008) 112–122.

[37] W. Parrish, J. Langford, Kluwer, Dordrecht, 1992, pp. 48–50.

[38] G.M. Sheldrick, Crystal structure re finement with SHELXL, Acta Crystallogr C71 (2015) 3–8.

[39] L.J. Farrugia, WinGX and ORTEP for windows: an update, J. Appl. Crystallogr. 45 (2012) 849–854.

[40] SAINT, Bruker AXS Inc., Madison, Wisconsin, USA, 2013.

[41] L.J. Farrugia, WinGX and ORTEP for Windows: an update, J. Appl. Cryst. 45 (2012) 849–854.

[42] A.L. Spek, Structure validation in chemical crystallography, Acta Crystallogr D65 (2009) 148–155.

[43] N. Dharmaraj, P. Viswanathamurthi, K. Natarajan, Ruthenium(II) complexes containing bidentate Schiff bases and their antifungal activity, Transition Met. Chem. 26 (2001) 105–109.

[44] Y. Anjuneyula, R.P. Rao, Preparation, Characterization and Antimicrobial Activity Studies on Some Ternary Complexes of Cu(II) with Acetylacetone and Various Salicylic Acids, Synth. React. Inorg. Met-Org. Chem. 26 (1986) 257–272.

[45] B.G. Tweedy, Plant extracts with metal ions as potential antimicrobial agents, Phytopathology 55 (1964) 910–914.

[46] N.A. Negma, M.F. Zakia, M.A.I. Salemb, Cationic schiff base amphiphiles and their metal complexes: surface and biocidal activities against bacteria and fungi, Colloids Surf. B: Biointerfaces 77 (2010) 96–103.

[47] A. Sahraei, H. Kargar, M. Hakimi, M.N. Tahir, Distorted square-antiprism geometry of new zirconium (IV) Schiff base complexes: synthesis, spectral characterization, crystal structure and investigation of biological properties, J. Mol. Struct. 1149 (2017) 576–584.

[48] A. Sahraei, H. Kargar, M. Hakimi, M.N. Tahir, Synthesis, characterization, crystal structures and biological activities of eight-coordinate zirconium(IV) Schiff base complexes, Transition Met. Chem. 42 (2017) 483–489.